Far-from-equilibrium film growth on alloy surfaces: Ni and Al on NiAl(110)

Yong Han, Dapeng Jing, Barış Ünal, P. A. Thiel, and J. W. Evans

Phys. Rev. B **84**, 113414 — Published 27 September 2011

DOI: 10.1103/PhysRevB.84.113414

Far-from-Equilibrium Film Growth on Alloy Surfaces: Ni and Al on NiAl(110)

Yong Han,[1,*] Dapeng Jing,[2,3] Barış Ünal,[3] P. A. Thiel,[2,3] and J. W. Evans[4,3]

[1] *Institute for Physical Research and Technology, Iowa State University, Ames, Iowa 50011*
[2] *Department of Chemistry, Iowa State University, Ames, Iowa 50011*
[3] *Ames Laboratory-USDOE, Iowa State University, Ames, Iowa 50011*
[4] *Department of Physics and Astronomy, Iowa State University, Ames, Iowa 50011*

STM analysis reveals diverse non-equilibrium island structures formed by deposition of Ni and Al on NiAl(110) at around 300 K. Epitaxial growth in this complex alloy system is described by multisite lattice-gas modeling incorporating DFT energetics for adatoms both at adsorption sites and transition states. This approach accounts for multiple adsorption sites and diffusion paths, and accurately describes diffusion/detachment kinetics for a vast number of step edge configurations. This is key for realistic description of island growth shapes, structure, and partial alloy ordering.

PACS numbers: 68.55.-a, 61.44.Br, 68.37.Ef, 81.15.Aa

Homoepitaxial growth of single-component metal films (A on A) leads to the development of a rich variety of complex far-from-equilibrium morphologies at lower deposition temperatures T in systems which have simple equilibrium states.[1,2] Such morphologies result from system-specific kinetic limitations on step edge or interlayer diffusion on the time-scale of film growth. Essentially the same behavior can be observed in heteroepitaxy (A on B) at least with low lattice misfit, whereas distinct strain-induced features occur for higher misfit.[3] Other studies of alloy overlayers and films (A+B on A or on C) have either focused on near-equilibrium short-range order[4,5] or on pattern formation reflecting interplay between chemical interactions and strain.[6] There has also been extensive interest in the competition during deposition between alloy ordering and either island growth[7–11] or kinetic roughening[12,13] often in the case where strain is not significant. Unfortunately, such investigations invariably used idealized models with generic Metropolis-type prescriptions of diffusion dynamics which cannot capture system-specific non-equilibrium behavior. This motivates development of new modeling approaches to describe, elucidate and ideally facilitate control of such complex behavior.

Rather than the single-component substrates employed in the above studies, use of binary alloy substrates provides new opportunities to guide the creation of thin film nanostructures with desired properties. However, analyses of film growth on binary alloys (A or B or B+C on BC) are rare,[14] particularly for far-from-equilibrium growth at low T with effectively frozen substrate dynamics.[15,16] Even for lattice-matched overlayers, there is significant additional complexity for alloy substrates such as multiple types of adsorption sites and diffusion pathways. This complicates description of edge diffusion and detachment which can occur for vast number of local step edge environments, especially for codeposition. Thus, a realistic atomistic-level description of non-equilibrium growth in such complex alloy systems pursued here requires a more general formalism than those used for simpler systems. Specifically, we apply multisite lattice-gas (LG) modeling together with a precise new algorithm and high-level energetics to determine all relevant diffusion barriers. Model behavior is then be assessed via kinetic Monte Carlo (KMC) simulation.

In this Report, we analyze submonolayer deposition of Ni and Al on NiAl(110) at around 300 K which produces far-from-equilibrium growth structures. Deposition of Ni or Al separately produces irregular island growth shapes, and stoichiometric codeposition produces deposition-protocol-dependent structures far from perfect equilibrium alloy ordering. Realistic multisite LG modeling is developed for this system with energetics guided by density functional theory DFT to accurately describe both thermodynamics (adsorption and interaction energies) and kinetics as described above. The latter is essential for realistic description of non-equilibrium evolution. A key goal of our modeling is to elucidate the fundamental process of alloy self-growth by simultaneous stoichiometric codeposition, including enhanced alloy ordering with increasing T.

Experimental details of NiAl(110) sample preparation and of the UHV chamber are described elsewhere.[15] Ni was evaporated from a commercial Mantis source and Al from a homemade source. Film morphologies were imaged with an Omicron VTSTM. In-plane sample orientation was checked by codeposition of Ag which forms bilayer islands elongated in the [001] direction.[15] Film composition and purity were checked with AES and XPS. Our DFT analysis used the plane-wave based VASP package within the generalized gradient approximation using the PAW approach and PBE functional (cf. Ref. 16).

Ni deposition at 300 K with flux $F = 0.003$ ML/s produces islands with a density of $\sim 4 \times 10^{-3}$ nm^{-2} at ~ 0.1 ML, and a height of $\sim$ 0.2 nm (with a weak tip bias dependence) corresponding to monolayer islands. Ni islands are rather irregular and on average elongated along the [001] direction at lower coverages. See Fig. 1(a). There is some preference for diagonal step edges. This feature is slightly enhanced for deposition at lower F, and at higher coverages [Fig. 1(b)]. For some regions of some islands, small bumps or protrusions of ~ 0.05 nm in height are apparent. We believe that these correspond to substrate defects overgrown by islands, noting that we

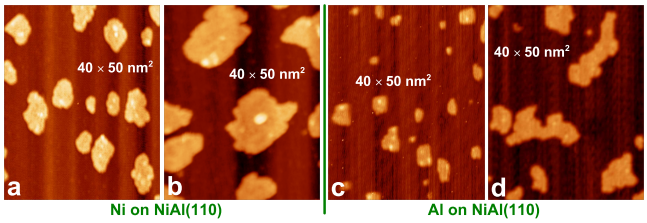

FIG. 1. (color online) STM images for deposition at 300 K: (a) 0.19 ML Ni ($F = 0.003$ ML/s); (b) 0.12 ML Ni ($F = 0.0003$ ML/s); (c) 0.10 ML Al ($F = 0.003$ ML/s); (d) 0.27 ML Al ($F = 0.009$ ML/s). The [001] direction is vertical.

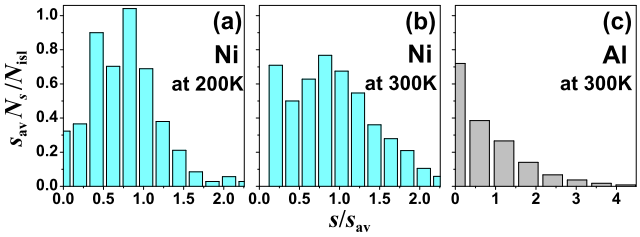

FIG. 2. (color online) Scaled island size distributions (ISD) at 0.2 ML for the density, N_s, of islands of s atoms, where $s_{\rm av}$ denotes the average size and $N_{\rm isl}$ the overall density.

will show that most islands are nucleated at defects.

Al deposition at 300 K with $F = 0.003$ ML/s produces islands with a density of $\sim 1 \times 10^{-2}$ nm^{-2} at ~ 0.1 ML which we claim mainly reflects the surface defect density. The measured island height of ~ 0.2 nm (-2 V) or ~ 0.3 nm ($+2$ V) has a strong tip bias dependence, but corresponds to monolayer islands. Smaller Al islands tend to be compact with a propensity for [001] steps, but islands become irregular during growth. See Figs. 1(c)–1(d). For typical islands, small bumps of ~ 0.05 nm in height are apparent sometimes throughout the island. While some could reflect overgrown defects, these bumps likely also reflect strain relief and structural variation occurring in Al islands, features not expected for Ni islands.

Island size distributions (ISD) shown in Fig. 2 provide insight into island nucleation. For homogeneous nucleation, the monomodal ISD progressively sharpens with the onset of reversibility. For Ni, the ISD instead broadens from 200 K to 300 K crossing this onset, suggesting significant heterogeneous nucleation at least at 300 K. For Al at 300 K, the ISD is monotonically decreasing indicating the dominance of heterogeneous nucleation, the ISD shape reflecting the spatial distribution of defects.

Next, we discuss anticipated and observed behavior for *codeposition* at 300 K of roughly equal amounts of Ni and Al (0.1–0.2 ML each) for typical fluxes $F \sim 10^{-3}$ ML/s. For such low T, one expects that these two-component nanostructures will have deposition-protocol-dependent configurations far from perfect equilibrium alloy order. Indeed, depositing first Al and then Ni produces monolayer islands with a robust Al core separated by a sharp interface from a Ni ring with irregular outer perimeter resembling pure Ni islands at 300 K. However, depositing first Ni and then Al produces a Ni core partly disrupted by the surrounding Al ring. Such core-ring structures, which we shall describe in detail elsewhere, should be expected for far-from-equilibrium growth,[17,18] despite counter claims.[10] In contrast, simultaneous stoichiometric codeposition at 300 K will produce very different mixed-component structures, as demonstrated below.

To develop a detailed atomistic-level understanding of these observations, we first consider the adsorption and diffusion of *isolated* adatoms on NiAl(110). Both Ni and Al prefer the Ni short bridge (Ni-br), although Ni resides at the Al short bridge (Al-br) in an equilibrated alloy film! Ni makes diagonal hops between neighboring Ni-br and Al-br sites, diffusing with an isotropic barrier of $E_d = 0.40$ eV. In contrast, Al diffuses preferentially in the [001] direction between Ni-br sites over on-top Ni sites with a barrier of $E_d = 0.30$ eV. Al can also hop in the [110] direction over Al-br sites with a barrier of $E_d = 0.51$ eV. See Fig. 3(a) for DFT adsorption energies at Ni-br and Al-br sites and at transition states (TS). For *aggregated* adatoms, we find a preference for "dense" islands with both Al-br and Ni-br sites populated, the cost of populating less favorable Al-br offset by enhanced adatom interactions. Also, Al diffusion along island edges occurs predominantly via diagonal hops [dashed yellow arrows in Fig. 3(a)] like Ni, a different pathway than for isolated Al [solid yellow arrows in Fig. 3(a)]. These features necessitate multisite LG modeling.

To prescribe *adlayer thermodynamics*, we assess from DFT the pair interactions between various types of adatoms at both types of adsorption sites for various separations. See Figs. 3(c)–3(d). Correct treatment of *non-equilibrium growth kinetics* also requires an accurate description of diffusion barriers for the various pathways above and for all local island edge configurations. To this end, we also assess pair interactions with one adatom at a TS and another at nearby adsorption sites. See Table I. Then, hopping barriers are determined from $E_{\rm act} = E_{\rm TS} - E_{\rm init}$, where $E_{\rm init}$ ($E_{\rm TS}$) is the total energy in the initial (transition) state. Both energies are obtained from a sum of the relevant adsorption energy and all pair interaction energies. See Fig. 3(b) for interactions impacting Ni diffusion along an alloy island edge. Detailed-balance is automatically satisfied[19]. Arrhenius hop rates with prefactors $\nu = 10^{13}$/s provide input to KMC simulation of an atomistic multisite LG model with adatoms at both Ni-br and Al-br sites. Deposition and hopping are implemented with the appropriate relative rates.

Our treatment has some limitations. DFT energies are not exact and adjusting some interactions better describes finer details of island shapes. We do not include many-body interactions, but pairwise contributions should dominate and are shown below to capture adlayer thermodynamics. Also, we do not account for strain buildup in growing islands, but do perform all DFT analyses on a fully relaxed substrate. However, "dense" Ni islands occupying both Ni-br and Al-br sites have little

TABLE I. Interactions in eV (attraction > 0) between adatoms with one adatom is at an adsorption site (Ni-br sites 1, 3, ...; Al-br sites 2, 4, ...) and another is at a TS (approximated as a Ni-top site t or Ni-Al bridge site b). See Fig. 2(a).

Ni(b)-Ni(3)	0.25	Al(b)-Al(3)	0.29	Ni(b)-Al(3)	0.71	Al(b)-Ni(3)	0.62	Al(t)-Al(2)	−1.00	Al(t)-Ni(2)	−0.44
Ni(b)-Ni(5)	0.14	Al(b)-Al(5)	0.40	Ni(b)-Al(5)	0.28	Al(b)-Ni(5)	0.24	Al(t)-Al(3)	−12.00	Al(t)-Ni(3)	−6.50
Ni(b)-Ni(6)	0.30	Al(b)-Al(6)	0.45	Ni(b)-Al(6)	0.85	Al(b)-Ni(6)	0.73	Al(t)-Al(4)	0.12	Al(t)-Ni(4)	0.06
Ni(b)-Ni(8)	0.18	Al(b)-Al(8)	0.20	Ni(b)-Al(8)	0.14	Al(b)-Ni(8)	0.18	Al(t)-Al(7)	0.02	Al(t)-Ni(7)	0.01

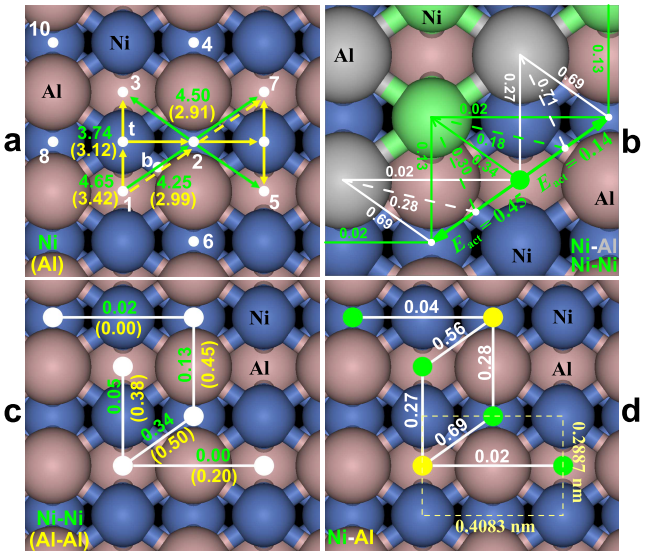

FIG. 3. (color online) (a) Ni-br and Al-br adsorption site and TS binding energies in eV for isolated Ni (Al) on NiAl(110); diffusion paths: green (yellow) arrows for Ni (Al); sites 1, 3, ... = Ni-br; 2, 4, ... = Al-br; t = Ni-top; b = Ni-Al bridge. (b) Ni diffusion along a diagonal Ni-Al island edge: solid (dashed) lines denote interactions of the diffusing Ni at adsorption sites (TS) with nearby adatoms. (c) Ni-Ni (Al-Al); (d) Ni-Al interaction energies in eV (attraction > 0). Dots denote adatoms or adsorption sites. [100] direction is vertical.

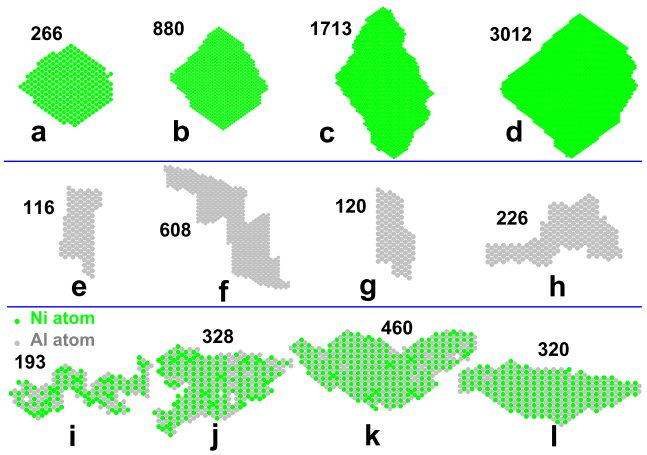

FIG. 4. (color online) Simulated islands (sizes in atoms). Ni at 300 K: (a)–(c) $F = 0.003$ ML/s; (d) $F = 0.0003$ ML/s. Al at 300 K: (e)–(f) $F = 0.003$ ML/s; (g)–(h) $F = 0.009$ ML/s. Simultaneous stoichiometric codeposition of Ni and Al ($F = 0.03$ ML/s) at: (i) 300 K; (j) 400 K; (k) 500 K; (l) 600 K.

lateral strain (the separation of neighboring Ni matches Ni(100) to within 0.2%; the areal compression relative to Ni(100) is less than 5%). Furthermore, ordered stoichiometric Ni+Al islands are also unstrained, where we note that these are particularly relevant for our analysis of simultaneous codeposition. On the other hand, "dense" Al islands do have compressive strain. This strain is relaxed locally by the Al atoms on Al-br sites sitting higher above the substrate than those on Ni-br sites. In addition, we should note that other more complex adlayer structures maybe be energetically competitive [cf. Au and Ag on NiAl(110)].[16,17] Thus, our modeling of Al islands may provide a simplified description of actual behavior. Finally, we have checked that exchange with the substrate and concerted terrace diffusion are energetically prohibitive at around 300 K, so we do not incorporate these processes into the modeling. (Even the thermodynamically preferred exchange of an Al adatom with an excess Ni atom in the surface layer has a barrier above 1 eV.)

First, we describe consequences of our model energetics for *adlayer thermodynamics*. The energy per adatom is lower for complete dense adlayers of Ni or of Al populating *both* Ni-br and Al-br sites than for complete dilute adlayers populating just Ni-br or just Al-br sites: −5.36 vs. −4.70 (Ni-br) or −4.65 eV (Al-br) for Ni; −4.68 vs. −4.00 (Ni-br) or −3.36 eV (Al-br) for Al. This in part reflects strong attractions between adatoms at diagonal nearest-neighbor (NN) Ni-br and Al-br sites. For mixed Ni+Al adlayers, perfect alloy ordering with Ni (Al) on the correct Al-br (Ni-br) sites has the lowest energy of −11.41 eV per Ni-Al pair. One obtains −10.30 eV per pair for perfect alloy ordering on the wrong sites, and −10.04 eV for phase-separated dense Ni and Al islands. This behavior in our pair interaction model tracks well results from direct DFT analysis incorporating (relatively insignificant) many-body contributions to the energetics for complete adlayers. "Diagonal" steps (with slopes of $\pm 1/\sqrt{2}$ reflecting the NiAl(110) rectangular unit cell) for dense Ni islands have significantly lower energies than the next most favorable horizontal and vertical steps. Thus, equilibrium shapes are distorted octagons with long diagonal steps. For dense Al islands, [100]-oriented steps with Al on Ni-br sites are most favored. For perfectly ordered Ni+Al islands, diagonal steps are preferred, so equilibrium shapes are similar to Ni islands.[20]

Now we turn to our central focus, the kinetics of island formation. For *nucleation and growth of Ni islands* mediated by almost isotropic terrace diffusion, the most stable dimer is a diagonal NN pair. The "bare" interaction strength is 0.34 eV, but since one Ni is at an Al-br site with weaker adsorption energy by 0.15 eV, the effective binding energy (relative to separated Ni on Ni-br sites) is $E_b = 0.19$ eV. This implies homogeneous nucleation is irreversible at 200 K, but reversible at 300 K.[2] Simulation of homogeneous nucleation in our atomistic model for a perfect surface yields an island density of 2.6×10^{-2} nm^{-2} at 200 K with $F = 0.001$ ML/s which is $\sim 50\%$ of experiment (with the same F). The simulated density at 300 K is only $\sim 20\%$ of experiment (at the same F). This reflects an increasing contribution of heterogeneous nucleation with increasing T. Island shapes are impacted by island density. Thus, in our shape studies, we seed the system with the appropriate island density or perform a single-island simulation in a small system with size matching the experimental area per island. Then, the model also recovers island shapes. See Figs. 4(a)–4(c) for growth at 300 K for $F = 0.003$ ML/s as in Fig. 1(a), and Fig. 4(d) for lower F as in Fig. 1(b). Edge diffusion is active along diagonal steps at 300 K with barrier $E_e \sim 0.35$ eV, but not along horizontal or vertical steps. Thus, edge atoms flow to the latter which "grow out" producing islands with a preference for diagonal steps. Vertical elongation reflects the feature that corner rounding of edge atoms from diagonal steps is easier to horizontal steps (at the top and bottom of the growing island) than to vertical steps.

Nucleation and growth of Al islands is mediated by strongly anisotropic terrace diffusion. The most stable dimer is vertically aligned on Ni-br sites with a binding energy of $E_b = 0.38$ eV, implying irreversible homogeneous nucleation at 300 K.[2] Note that the stronger "bare" interaction for a vertical dimer on Al-br sites is offset by a large adsorption site penalty, so this dimer is not stable. The simulated island density at 300 K is far below experiment reflecting the dominance of heterogeneous nucleation (which is likely also irreversible). However, simulations imposing experimental island densities do recover trends in experimental island shapes, i.e., a tendency for [001] steps at least in smaller islands, and irregular growth of larger islands. See Figs. 4(e)–4(h). Note that in simulations incorporating only the vertical and horizontal diffusion pathway for isolated Al, edge diffusion becomes effectively inoperative at 300 K producing highly ramified fractal islands. Edge diffusion via diagonal hops, especially along vertical edges ($E_e \sim 0.5$ eV), facilitates formation of the island structures seen in experiment.

Next, we discuss simulation results for *codeposition*. Our model recovers the expected and observed island core-ring structures formed by sequential deposition. However, our focus here is on the fundamental process of alloy self-growth via *simultaneous stoichiometric codeposition* of Ni and Al. Specifically we utilize our model to present the first realistic treatment of the extent of ordering versus deposition temperature. (Note that atomic-resolution STM imaging of such local ordering is difficult.) Thermodynamically favored perfect ordering should be achieved at high enough T. However, at 300 K, our simulations reveal intermixing, but poor alloy ordering. Significantly, the degree of alloy ordering increases quickly with T, so that near-perfect ordering is achieved by 600 K (far below the bulk NiAl melting point of 1640 K). Despite this feature, the island shape at 600 K is still far from the distorted octagonal equilibrium form described above.[20] See Figs. 4(i)–4(l).

In summary, deposition of Ni and Al at 300 K on NiAl(110) produces a rich variety of far-from-equilibrium nanostructures. Multisite LG modeling incorporating DFT-guided energetics for both interactions and barriers is essential in enabling a realistic treatment of their growth kinetics. This includes description of both growth shapes and the T-dependence of alloy ordering. This approach has general applicability for epitaxial alloy systems with low strain.

This work was supported by NSF Grant CHE-1111500 with NERSC computational resources. Ames Laboratory operated under Contract No. DE-AC02-07CH11358.

* Email: octavian2009@gmail.com

[1] T. Michely and J. Krug, *Islands, Mounds, and Atoms* (Springer, Berlin, 2004).
[2] J. W. Evans et al., Surf. Sci. Rep. **61**, 1 (2006).
[3] R. Q. Hwang and M. C. Bartelt, Chem. Rev. **97**, 1063 (1997).
[4] H. Hartmann et al., Surf. Sci. **603**, 1439 (2009).
[5] M. Chen et al., Science **310**, 291 (2005).
[6] G. E. Thayer et al., Phys. Rev. Lett. **89**, 036101 (2002).
[7] M. Kotrla et al., Phys. Rev. B **62**, 2889 (2000).
[8] T. Volkmann et al., Surf. Sci. **586**, 157 (2005).
[9] S. Weber et al., J. Phys.: Cond. Mat. **20**, 265004 (2008).
[10] F. Dumont et al., Phys. Rev. B **77**, 153404 (2008).
[11] M. Einax et al., Phys. Rev. Lett. **99**, 016106 (2007).
[12] J. R. Smith and A. Zangwill, Phys. Rev. Lett. **76**, 2097 (1996).
[13] E. N. Oskoee et al., Phys. Rev. E **69**, 061606 (2004).
[14] J. P. Pierce et al., Phys. Rev. Lett. **99**, 026101 (2007).
[15] Y. Han et al., Phys. Rev. Lett. **100**, 116105 (2008).
[16] Y. Han et al., Phys. Rev. B **81**, 115462 (2010).
[17] T. Duguet et al., Proc. Nat. Acad. Sci., in press.
[18] M. C. Bartelt, et al., Phys. Rev. Lett. **81**, 1901 (1998).
[19] For Al hopping, the true TS could be an initial or final unstable Al-br site, a feature checked for each Al hop.
[20] Our model predicts an equilibrium shape with the lengths of "diagonal, vertical, and horizontal steps in the proportions 3.78 : 1.59 : 1.